CIRP Annals - Manufacturing Technology 71 (2022) 441–444

Contents lists available at ScienceDirect

CIRP Annals - Manufacturing Technology

journal homepage: https://www.editorialmanager.com/CIRP/default.aspx

One step machining of hierarchical optical structures for autostereoscopic images

Yaoke Wang, Ping Guo*

Department of Mechanical Engineering, Northwestern University, Evanston, IL, USA

ARTICLE INFO

Article history:
Available online 28 April 2022

Keywords:
Optical
Cutting
Autostereoscopy

ABSTRACT

This work presents a new optical design and the corresponding novel machining strategy to achieve the one step generation of hierarchical optical structures on a flat surface for autostereoscopic effects. The hierarchical structures combine V-groove arrays as a parallax barrier for stereopsis and integrated diffraction gratings with variable grating spacing for motion parallax. The multi-scale surface structures are machined simultaneously using the tool geometry to form V-grooves while utilizing elliptical tool vibration to generate blazed gratings concurrently. An autostereoscopic image with strong depth perception is fabricated with a pixel density exceeding 1,660 pixels per inch.

1. Introduction

Fabrication of autostereoscopic three-dimensional (3D) images attracts great interest for their existing and emerging applications, including functional decoration, virtual and augmented reality, anti-counterfeiting, and packaging [1]. Autostereoscopic images provide "naked-eye" 3D effects without the need of any viewing gears. The 3D perception is achieved based on ***stereopsis***, which presents two different perspective images for the left and right eyes, and ***motion parallax***, which changes object orientations when viewed from different angles. The combined effects help to "deceive" human eyes and achieve a realistic stereoscopic effect.

Autostereoscopic images rely on engineered optical structures, which are often desirable to be easily replicated through optical molding, embossing, or transfer printing for mass production. However, the manufacturing of the master optical mold is still challenging to date.

Holography is the most iconic technology for passive autostereoscopy that reconstructs the light field of a 3D scene observed from different perspectives with wavefront information recorded on a physical medium. Early rainbow holograms can achieve both stereopsis and horizontal parallax under only white light illumination instead of a coherent light source, but they require a physical object for analog holographic recording. With the development of computer-generated holograms and holographic stereograms [2], the state-of-the-art holograms can display 3D images with full-color stereopsis and motion parallax from hundreds of pre-recorded perspective views [3]. However, the fabrication of master holograms can only work with photopolymers using a spatial light modulator or direct writing of fringe patterns. Furthermore, the options for mass replication of holograms are even further limited. The reflection volume-type holograms cannot be transferred to a master metal mold, while the transmission fringe-type holograms can be transferred to a nickel shim by multi-step electroforming [4], at the expense of significant brightness reduction and quality degradation.

Ultraprecision machining (UPM) of optical molds has demonstrated excellent form accuracy and nanometric surface quality [5]. UPM works directly on nickel-phosphorus coatings, which eliminates mold transfer in the replication of holograms. Some promising results have demonstrated the application of UPM in the fabrication of lens arrays [6, 7], optically variable devices [8], and diffractive optics [9]. Particularly, one can utilize machined lenticular arrays to achieve stereopsis and micro-lens arrays for integral imaging to achieve motion parallax. However, a complex multilayer design is needed, which adds to system complexity and fabrication cost. Moreover, previous UPM-based methods have only demonstrated the ability to realize either stereopsis or motion parallax, unable to match the quality of a holographic stereogram. The limitation of UPM in machining complex surface features has limited the optical design flexibility to achieve fully autostereoscopic images. Inspired by the vibration-induced grating features in UPM [10], we explore the new idea of using both tool geometry and trajectory to machine multi-level structures simultaneously and their application in autostereoscopy.

This paper presents a new optical design of hierarchical optical structures on a flat surface to achieve autostereoscopy 3D vision with both stereopsis and motion parallax, as well as the corresponding novel manufacturing technique, based on vibration-assisted UPM, to achieve one step machining of the designed multi-scale structures. The optical design novelty lies in the hierarchical structure design, which is composed of V-groove arrays as a parallax barrier and integrated variable blazed gratings to achieve diffraction-based image reconstruction. The new manufacturing technique achieves simultaneous generation of two-level surface structures at very different length scales (50 μm vs. 500 nm) by utilizing both the tool geometry for V-groove shaping and the elliptical tool vibration [10] for grating

Submitted by Jian Cao, Northwestern University, IL, USA
* Corresponding author.
E-mail address: ping.guo@northwestern.edu (P. Guo).

https://doi.org/10.1016/j.cirp.2022.04.041
0007-8506/

generation. The proposed design and manufacturing strategy make it possible to directly and efficiently machine master optical molds for mass production while providing high-quality autostereoscopic images unachievable by current UPM-based methods. Detailed theoretical analyses of the optical design and manufacturing strategies are presented. Finally, the simulation and experimental results are compared to demonstrate the autostereoscopic effect.

2. Methodology

2.1. Hierarchical optical structure design

A hierarchical optical structure design is proposed to store the visual information for image reconstruction, stereopsis, and motion parallax. The design comprises V-groove arrays and integrated optical elements with variable blazed gratings.

As a demonstration case shown in Fig. 1(a), we create a 3D model of a bird holding a Northwestern tag in its beak. A pencil is added in the depth direction, pointing to the tag to increase the parallax effect. The stereoscopic view of the bird is rendered in pairs with a constant horizontal angle α between the two views to represent the scenes seen by the left and right eyes, respectively. Next, five pairs of images (1L/1R to 5L/5R) are rendered with five vertical viewing angles β from low to high to represent the different perspective views for vertical parallax. Then, the ten rendered images are combined into a single composed image, as shown in Fig. 1(a). The basic spatial unit in the composed image is an optical element at location (i, j), which is composed of subpixels (i, j) at the same location from all ten perspective views, similar to the concept of a "hogel" in the hologram.

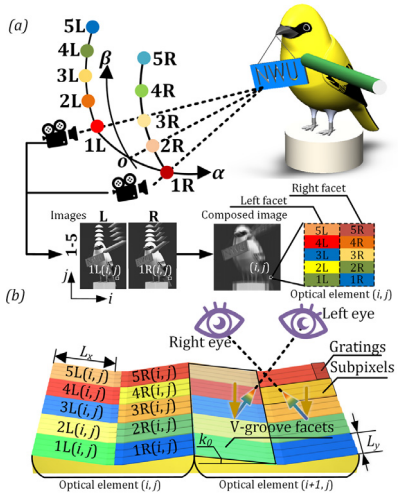

Fig. 1. (a) Acquisition and composition of parallax images of a 3D model from different perspectives; and (b) schematics of hierarchical surface structure design on a flat surface displaying autostereoscopic effects.

The detailed configuration of an optical element and its topological relationship with the V-grooves are further illustrated in Fig. 1(b). Each optical element at (i, j) contains two facets of the V-groove, where the left facet is composed of subpixels $1L(i, j)$–$5L(i, j)$ while the right facet consists of subpixels $1R(i, j)$–$5R(i, j)$. The color coding indicates that each subpixel, with a width L_x and a length L_y, stores the graphic information with a unique grating spacing d, depending on the image grayscale values and the viewing angles α and β in the particular perspective view.

The reconstruction of different perspective views utilizes the combination of deflection and diffraction variations as the observation direction changes. The top-level V-groove arrays act as a parallax barrier to achieve a stereoscopic view. They are designed with a groove angle k_0 to decouple the diffraction angles from the two facets to two different directions. As a result, the observer's left and right eyes receive two separate image reconstructions, forming stereoscopic depth perception. To further enhance the depth cue, each facet of V-grooves contains five subpixels. Each subpixel of the optical element is from the image of a different perspective view of the object to enable the diffraction decoupling for vertical parallax by assigning variable grating spacing. The design functions similar to an optically variable device, so the observer will only see a particular perspective view depending on the vertical observation angle. In addition, the pixelated blazed gratings are asymmetrically integrated on the two V-groove facets, which are used to achieve the separate reconstruction of images for two eyes by diffraction-based structural coloration.

An optical simulation is developed on MATLAB to verify the design of autostereoscopic images. The optical simulation extends a nonparaxial scalar diffraction theory [11] and considers the multi-scale 3D surface features, including the V-grooves for stereoscopic view, variable grating spacing for motion parallax, and the predicted 3D grating profile (details introduced in Section 2.2) for more accurate diffraction simulation.

Since the stereo decoupling is pre-determined by the groove angle k_0, the horizontal rotation angle is set to k_0 and $-k_0$ to simulate the observed image from the two eyes. The geometry parameters of the simulation are defined in Table 1. It is worth mentioning that the k_0 is set to 8° because the viewing angle difference between the two eyes is about $2k_0$ or 16° when observed at a distance of 200 mm. L_x and L_y are collectively determined by the resolution of captured images and the dimension of the machined image.

Table 1
Summary of simulation parameters.

Groove angle	$k_0 = 8°$	Subpixel width	$L_x = 25\ \mu$m
Blaze angle	$\gamma_0 = 10°$	Subpixel length	$L_y = 12\ \mu$m
Red wavelength	$\lambda_{red} = 600$ nm	Violet wavelength	$\lambda_{vio} = 400$ nm
Increment of viewing angles in the vertical direction	$\Delta\beta = 2°$		

The simulated images to demonstrate stereoscopic view are presented in Figs. 2(a)–2(c), where the two eyes receive two decoupled images from two perspectives to form the stereo vision.

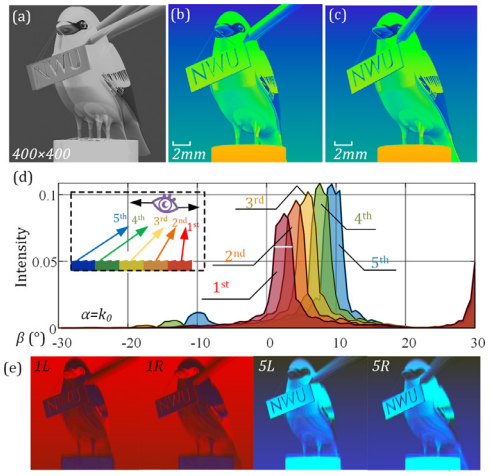

Fig. 2. (a) A composed image overlapping a stereo pair from the simulated observation from (b) the left eye ($\alpha = -8°$, $\beta = 10°$) and (c) the right eye ($\alpha = 8°$, $\beta = 10°$); (d) diffraction intensity distribution of 532 nm incident light; and (e) full image simulation of stereopsis (L vs. R) and motion parallax (1 vs. 5).

For the motion parallax, different perspective views due to the change of vertical viewing angle β are achieved based on the decoupling of diffraction peaks in different viewing angles. For example, as shown in Fig. 2(d), when the incident light wavelength is assumed to be 532 nm, the diffraction intensity will show five sequential peaks as the vertical viewing angle β increases. The grating spacing, d_k, and ultimately the cutting velocity at the subpixel k, v_k, is related to the subpixel grayscale value V_k and the observation angle, as defined by

$$v_k = d_k/f = \frac{\lambda_{red} - (1 - V_k)\lambda_{vio}}{f\sin 2(\gamma_0 + (k-1)\Delta\beta)} \quad (1)$$

Eq. (1) is an extension to the classical grating equation in the Littrow configuration [10]. The nominator converts the grayscale value V_k from the kth perspective image to a visual wavelength. The

denominator defines the observation angle, which starts from $2\gamma_0$ (blaze angle) and increases incrementally by $\Delta\beta$ for each perspective view to achieve motion parallax.

According to Eq. (1), the grating spacing ranges are 1170–1754 nm for d_1 and 850–1278 nm for d_5. Since the gratings with different spacings have individual optimized diffraction angles, each perspective view will be sequentially dominant with the change of observation angle, giving motion parallax to enhance the stereoscopic perception.

The full image simulations, including stereopsis and motion parallax, are presented in Fig. 2(e) for 1L,1R, 5L, 5R. To be noted, the simulation results consider the averaging effects from all subpixels of the ten images, so the overall color shows a more monochromic tone and a shift from red to blue in the different perspective views.

2.2. One step machining of hierarchical structures

In order to enable the efficient manufacturing of designed hierarchical optical structures, a novel manufacturing technique is proposed for one step machining of multi-scale surface features. The process schematics are illustrated in Fig. 3. The cutting tool (single crystal diamond) geometry is designed as a triangular shape with two straight cutting edges to match the groove angle of k_0. The two cutting edges are used to form the groove facet. Elliptical vibrations are added to the cutting tip during the ruling of V-grooves to concurrently generate diffraction gratings orthogonal to the cutting direction. The schematics of grating formation in the cutting plane are shown in Fig. 3(c). When the tool vibration frequency is fixed, the grating spacing d is proportional to the nominal cutting velocity. Thus, the grating spacing can be tuned by continuously changing the nominal cutting velocity to render variable grating spacing in each optical element.

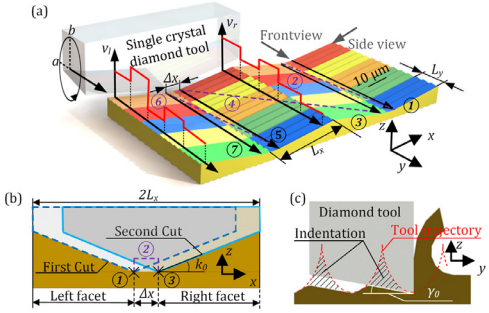

Fig. 3. One step generation of hierarchical optical structures: (a) process overview; (b) front view showing the sequential cutting of V-grooves; and (c) grating formation and indentation in the cutting plane.

In order to fabricate two facets of the V-grooves with different grating designs for the stereoscopic view, a sequential cutting strategy with a crossfeed offset, Δx, is proposed, as shown in Fig. 3(a). The first cut ① generates the left facet with a width L_x but also produces the gratings on the right facet simultaneously. The tool then retracts and translates with a crossfeed offset of Δx in ②. Due to this offset, the second cut ③ only machines the right facet to replace existing gratings with a brand-new layer of gratings belonging to the right facet, leaving the previously generated left facet intact, as shown by the front view of the process in Fig. 3(b). The process is repeated (④–⑦) for each V-groove, resulting in a V-groove array on the machined surface. By following this sequential cutting strategy, asymmetrical grating designs are engraved on the two facets of a V-groove independently so that the diffracted images from the two facets are completely decoupled for a stereoscopic effect.

The integrated blazed gratings are concurrently generated during the ruling of V-grooves with an elliptical vibration trajectory [10]. The combined motion of elliptical vibration and translation of the tool tip leaves periodic markings on the machined surface to form blazed gratings. It is worth noticing that the actual machined grating profile is different from the tool trajectory because of the interference of the tool flank and the undulating surface profile, as shown in Fig. 3(c). The working facet of the grating profile is indented by the tool flank, so the resultant blaze angle is equal to the tool clearance angle γ_0.

The surface profile of the hierarchical optical structure is numerically calculated with the coordinate definition shown in Fig. 3. The y-axis is aligned with the nominal cutting direction, while the z coordinates represent the surface profile height. By taking into account both the cutting and indentation process during each vibration cycle, the surface profile of a single vibration-induced grating in the y-z plane can be represented by:

$$z(y) = min\{\begin{matrix} -\tan(\gamma_0)\cdot(y-y_0) \\ \Gamma^{-1}(y) \end{matrix} \quad (2)$$

where $y_0 \forall [0, y]$, which indicates that traversing all points from 0 to y is required to calculate the height z at y. The tool trajectory function Γ describes the combined elliptical vibration and nominal cutting motion, which is given by

$$y = \Gamma(z) = \frac{d_k}{2\pi}\cos^{-1}\left(\frac{z}{b}\right) + a\cdot sin\left(\frac{1}{2\pi}\cos^{-1}\left(\frac{z}{b}\right)\right) \quad (3)$$

where d_k is the subpixel grating spacing from Eq. (1). a and b are the vibration amplitudes defined in Fig. 3(a).

Similarly, the surface profile in the x-z plane is consistent with the tool cutting edge if the minor offset Δx is neglected. The complete 3D surface profile is the combination of the grating profile in the y-z plane and the groove geometry in the x-z plane, which can be represented by

$$z(x,y) = tan(k_0)|x| + z(y) \quad (4)$$

The obtained detailed 3D profile $z(x, y)$ of the hierarchical optical structure is applied to the designed optical simulation presented in Section 2.1 to verify the stereopsis and motion parallax.

3. Experimental verification

Based on the optical design and simulation results, the bird design is machined using an ultra-precision lathe (Nanoform X, Precitech, USA) with three linear axes (X, Y, Z), where the nominal cutting velocity is controlled by Y-axis. The elliptical vibration trajectory, with the amplitudes of a = 0.5 μm and b = 1.5 μm, is generated using a custom-designed elliptical vibration tool. The tool vibration frequency is set to 2 kHz. We choose our elliptical vibration tool over a commercially available fast tool servo (FTS) since a well-tuned 2D vibration trajectory is critical to the grating formation quality, especially the aspect ratio [12], while an FTS can only provide longitudinal motion. Furthermore, an ultrasonic elliptical vibration tool can further improve the process efficiency by 10 folds, which operates above 20 kHz, far beyond the bandwidth of an FTS. The workpiece material is 260 brass. The triangular single crystal diamond tool is from Chardon Tool, USA. A close-up view of the machine setup is shown in Fig. 4(a). The nominal depth of cut is set to 4 μm, while the crossfeed is alternating between $2L_x$ (50 μm), the optical element width, and the crossfeed offset Δx (5 μm). Other geometric and process parameters are kept consistent with the simulation.

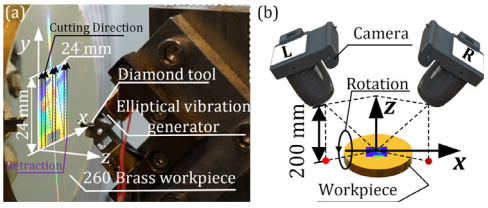

Fig. 4. (a) Experimental setup and (b) measurement configuration.

The designed observation distance is set to be 200 mm, which is defined by the average interpupillary distance divided by the V-groove angle ($2 \times k_0$). The image size is set to 24 mm × 24 mm. The adopted subpixel size (25 μm × 12 μm) results in a pixel density of over 1,660 pixels per inch (PPI), which is comparable to the state-of-

the-art holographic stereograms. In order to control grating spacing reliably at such a small length scale, the cutting velocity is continuously tuned by position-velocity-time interpolated motion. Due to the high efficiency of the proposed one step fabrication method for the hierarchical structures, the total machining time is within 3 h. The photo of the machined sample is shown in Fig. 5(a). The microscopic view of the machined surface, measured by NewView 7300 (Zygo, USA), is given in Fig. 5(b), clearly showing the groove facets and the integrated gratings. The randomly distributed defects in the photo are not induced by the vibration machining but pre-existing in the raw workpiece material. The measured surface profile of V-grooves is plotted in Fig. 5(c), which matches the design parameters summarized in Table 1. Since the tool has a micron-level nose radius, there is often a spike observed at the facet intersection. This part is not involved in image reconstruction, so the visual quality is not affected.

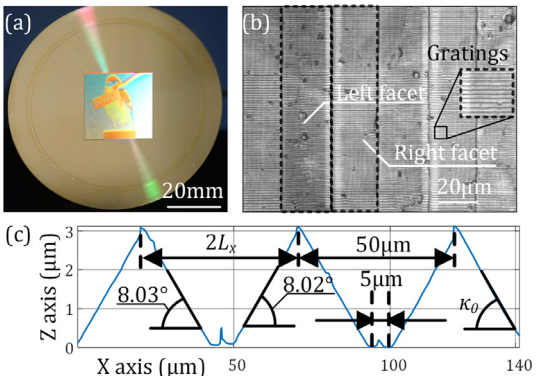

Fig. 5. (a) Machined workpiece; (b) microscope image of the machined surface; and (c) measured V-groove surface profile.

In the optical evaluation procedure shown in Fig. 4(b), the camera locations are back-calculated according to the designed observation angles α and β. The camera viewing distance is kept at 200 mm. The results of captured images are compared with the designed images in Fig. 6. The experimental results show a very good decoupling effect, so only one particular perspective image can be viewed at the designated viewing angle. The stereo pair images (L vs. R) present two slightly different views to the left and right eyes to give the depth cue (noticing the change of pencil orientations in the left and right views). The five perspective pairs (1 to 5) are selectively displayed depending on the viewing angle to provide motion parallax. The bird is slightly rotated in different perspective images, while the change of pencil orientation is more obvious to notice.

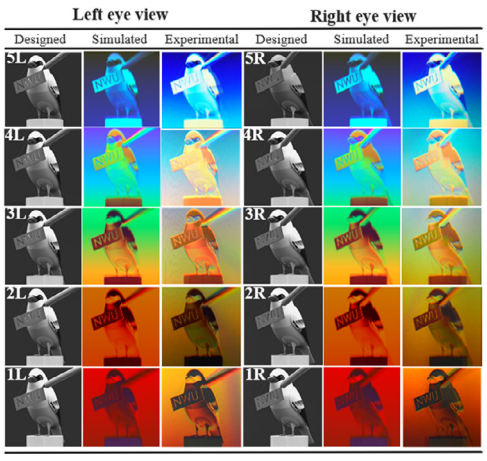

Fig. 6. Comparison between the designed perspective images, simulated and experimentally captured images. Notice the stereoscopic difference between the L and R images and motion parallax reflected by the image difference from 1 to 5, especially the change of pencil orientation.

4. Conclusion

This work presents a new hierarchical optical structure design on a planar surface to achieve autostereoscopic effects, which utilizes V-groove arrays to provide a stereoscopic view and integrated variable diffraction gratings to achieve structural coloration and motion parallax. We demonstrate the new process capability of UPM in one step generation of designed multi-scale surface structures. The elliptical tool vibration is utilized to realize concurrent grating generation, while the tool shape is designed to form the V-grooves. We have successfully demonstrated the machining of an autostereoscopic image with strong depth perception at a surface generation rate of 3.2 mm^2/min with a pixel density exceeding 1,660 PPI. To give a comparison, the latest iPhone 13 has a screen resolution equal to 460 PPI. The demonstrated technology and results might open up new opportunities in optical surface design and fabrication in augmented and virtual reality. Our future work will expand the number coded perspective views to provide a smoother transition effect as well as potential orthogonal cutting strategies to generate 2D gratings to realize full motion parallax.

Declaration of Competing Interest

The authors declare that they have no known competing financial interests or personal relationships that could have appeared to influence the work reported in this paper.

Acknowledgments

This work is supported by the start-up fund from McCormick School of Engineering, Northwestern University, Evanston, IL, USA.

References

[1] Holliman NS, Dodgson NA, Favalora GE, Pockett L (2011) Three-dimensional displays: a review and applications analysis. *IEEE Trans Broadcast* 57/2:362–371.
[2] Su J, Yan X, Huang Y, Jiang X, Chen Y, Zhang T (2018) Progress in the synthetic holographic stereogram printing technique. *Applied Sciences* 8/6:851.
[3] Fachada S, Bonatto D, Lafruit G (2021) High-quality holographic stereogram generation using four Rgbd images. *Appl Opt* 60/4:A250–A2A9.
[4] Behrens BA, Krimm R, Jocker J, Reithmeier E, Roth B, Rahlves M (2013) Method to Emboss Holograms into the surface of sheet metals. *Key Eng Mater* 549:125–132.
[5] Zhang X, Huang R, Kumar AS, Liu K (2018) High-efficiency swinging-rotating diamond shaping of fresnel lenses on roller molds. *CIRP Ann* 67/1:121–124.
[6] Pang K, Song L, Fang F, Zhang Y, Zhang H (2016) An imaging system with a large depth of field based on an overlapped micro-lens array. *CIRP Ann* 65/1:471–474.
[7] Tong Z, Zhong W, To S, Zeng W (2020) Fast-tool-servo micro-grooving freeform surfaces with embedded metrology. *CIRP Ann* 69/1:505–508.
[8] Guo P, Yang Y (2019) A novel realization of diffractive optically variable devices using ultrasonic modulation cutting. *CIRP Ann* 68/1:575–578.
[9] Brinksmeier E, Riemer O, Gläbe R, Lünemann B, Kopylow C, Dankwart C, Meier A (2010) Submicron functional surfaces generated by diamond machining. *CIRP Ann* 59/1:535–538.
[10] Yang Y, Pan Y, Guo P (2017) Structural coloration of metallic surfaces with micro/nano-structures induced by elliptical vibration texturing. *Appl Surf Sci* 402:400–409.
[11] Harvey JE, Vernold CL, Krywonos A, Thompson PL (1999) Diffracted radiance: a fundamental quantity in nonparaxial scalar diffraction theory. *Appl Opt* 38/31:6469–6481.
[12] Wang J, Wang Y, Zhang J, Yang Y, Guo P (2021) Structural coloration of non-metallic surfaces using ductile-regime vibration-assisted ultraprecision texturing. *Light: Advanced Manufacturing* 2/4:1–12.